IEEE Access
Multidisciplinary | Rapid Review | Open Access Journal

Received February 26, 2020, accepted March 21, 2020, date of publication March 26, 2020, date of current version May 8, 2020.

*Digital Object Identifier 10.1109/ACCESS.2020.2983523*

# Validation and Testing of Initial and In-Situ Mutual Coupling-Based Calibration of a Dual-Polarized Active Phased Array Antenna

**RODRIGO M. LEBRÓN[1,2], (Student Member, IEEE), PEI-SANG TSAI[3], (Member, IEEE), JONATHAN M. EMMETT[3], CALEB FULTON[1,2], (Senior Member, IEEE), AND JORGE L. SALAZAR-CERRENO[1,2], (Senior Member, IEEE)**

[1]School of Electrical and Computer Engineering, The University of Oklahoma, Norman, OK 73019, USA
[2]Advanced Radar Research Center (ARRC), The University of Oklahoma, Norman, OK 73019, USA
[3]Earth Observing Laboratory (EOL), National Center for Atmospheric Research (NCAR), Boulder, CO 80307, USA

Corresponding author: Jorge L. Salazar-Cerreno (salazar@ou.edu)

This work was supported in part by the National Center for Atmospheric Research (NCAR) through the Airborne Phased Array Radar (APAR) Development and Risk Mitigation Project (2017-2019).

**ABSTRACT** This paper presents experimental results of an initial and in-situ mutual coupling calibration techniques of an active phased array antenna. The antenna is a dual-polarized 64-element C-band subarray panel equipped with an RF beamformer that enables mutual coupling measurements. Both techniques were implemented, tested and validated using a custom anechoic chamber and a radar backend. The implementation of a radar backend enables the in-situ validation of both methods. A conventional near-field calibration procedure, also known as park and probe, was used as a reference, in order to validate the proposed method. To quantify the calibration effectiveness of the mutual coupling-based techniques, the results are translated into phase and amplitude errors. It is found that the amplitude estimation of the tested initial technique is affected by edge effects, resulting in errors larger than 1 dB, whereas the phase estimation is less sensitive, yielding an overall root mean square error (RMSE) of 2.5°. In contrast, the proposed in-situ technique is not affected by edge effects, and its estimation RMSE is less than 0.12 dB in amplitude and less than 0.75° in phase. Mutual coupling-based calibration techniques are demonstrated to be very versatile, as they provide calibration methods for environments outside an anechoic chamber, and they also enable immediate feedback on the health of the system.

**INDEX TERMS** Active phased array, calibration, component failure, mutual coupling, park and probe.

## I. INTRODUCTION

The National Center for Atmospheric Research (NCAR) is currently investigating the technical requirements for the next-generation airborne phased array radar (APAR). This airborne radar system will be used to retrieve dynamic and microphysical characteristics of clouds and precipitation [1]. Phased array radar (PAR) characteristics as sidelobe level, gain and beam accuracy are critical to the weather observation requirements [2], [3]. To ensure the performance of the radar, it is essential to develop a calibration scheme for a phased array radar system that is applicable during field operations. While the conventional method in an anechoic chamber is the baseline of any PAR calibration, development of a self-calibration method will provide additional calibration capability once the system is fielded. Calibration during field operations often requires minimum infrastructure and equipment. To comply with this limitation, the mutual coupling-based approaches are selected for further investigation.

Phased array calibration is the procedure to quantify the phase and amplitude misalignment among the active antenna elements [4]–[6]. These misalignment errors are due to hardware imperfections, namely component aging and differences in the electrical lengths of the microwave path between antenna elements. The objective of a phased array antenna calibration is to sample each antenna element in the array, and compare the obtained results to identify the differences in excitation among the elements. Phased array calibration

The associate editor coordinating the review of this manuscript and approving it for publication was Mohammad Tariqul Islam.

can be classified in two main types, initial and in-situ [7], [8]. As the name suggests, initial calibration is the first alignment check performed on the phased array system, whereas, in-situ calibration refers to the one performed on the operation location.

Initial calibration is performed immediately after fabrication of the system. It is often performed under controlled conditions of temperature and humidity inside of an anechoic chamber [9]. An example of this is the widely known park and probe technique [10], [11], that employs a robotic scanner. Other examples that require external equipment are [12]–[15]. In contrast, there are also techniques that take advantage of the inherent property of mutual coupling among elements of the array, and use it to avoid the employment of external equipment. This approach was pioneered by [16], and continued by [17]–[19]; even modern mmWave phased array prototypes for 5G applications started to embrace this calibration mechanism [20].

On the other hand, in-situ calibration attempts to correct misalignment that may emerge during operation of the system. This requires feedback measurements on location, wherever this may be. Oftentimes, it is not advisable or even possible to deploy external equipment for calibration purposes. As a result, it is preferable to use techniques that are self-contained as the ones mentioned in the previous paragraph, which are based on mutual coupling measurements, or techniques that employ built-in specialized feedback mechanisms to directly inject a test signal into the feed of the antenna elements [21]. Moreover, there are other mutual coupling-based techniques, developed specifically for in-situ applications, which rely on the results obtained by initial calibration. Examples of this are [7], [18], [22], [23], which employ embedded elements that monitor the current state of the array, and compare the results with the ones initially obtained; any difference between current and initial states is considered a misalignment.

The traditional park and probe technique, although a reliable method, is not always feasible to implement due to the need to set up a robotic scanner to sample a phased array system. Also, the mechanical movement required by the park and probe technique makes it time-consuming when compared to mutual coupling-based types, which are orders of magnitude faster. As a consequence, mutual coupling-based techniques seem more convenient and quite versatile in comparison with the park and probe calibration technique. However, mutual coupling-based calibration procedures rely on assumptions that may compromise their performance, casting doubts on the accuracy of their estimations. In this context, this work presents an experimental validation of both initial and in-situ calibration techniques. The goal is to evaluate the misalignment estimation accuracy of state-of-the-art mutual coupling-based techniques on an $8 \times 8$ active phased array radar. The evaluation is accomplished by comparing the results obtained using mutual coupling-based techniques, with results obtained using the park and probe technique.

For the initial technique case, the mutual coupling-based method proposed and simulated by Bekers *et al.* [19], and mathematically formulated in Mitchell [24], is implemented. This resourceful approach is capable of using the coupling among several different pair of elements to compute a least square minimum error estimate of the phase and amplitude difference between them. However, the approach may suffer biases caused by the discontinuities inherent to elements near the edge. Thereby, the feasibility of this technique is unknown for small size array cases. The motivation behind the selection of this technique is that, to the authors' knowledge, it has not been experimentally validated yet, and its performance on arrays of small sizes is to be determined. Moreover, to serve as a comparison reference, the reliable park and probe technique has also been tested as an initial type.

For the in-situ case a hybrid mutual coupling-based technique has been proposed and tested. The proposed in-situ technique is derived from the work of Şeker [18] and has been modified to track changes between the current state of the array and its initial state. The hybrid technique is motivated by the need of using only mutual coupling measurements between the active elements of the array, avoiding the implementation of embedded elements which are required by the original change tracking approach.

Furthermore, there is also a constant threat of element failure [25], which will compromise the mutual coupling-based calibration efforts, and it can adversely affect the resulting pattern. Thus, it is important to determine whether or not an element has failed. Fortunately, mutual coupling-based techniques not only allow one to quantify phase and amplitude misalignment, but their raw results by themselves contain information about the health of active element components. In case of component failure, the collected coupling data can be analyzed to determine failed active elements, and also to identify which component have failed. For this reason, this work also describes how the raw coupling data was interpreted in order to quickly diagnose failed components.

The paper is organized as follows: Sections II and III introduce the theory of the initial and in-situ techniques, respectively, that were implemented. Section IV describes the experimental setup, including a description of the device under test (DUT) and the instrumentation. In Section V the experiments are detailed, and results are presented and discussed. Finally, the conclusion is given in Section VI.

## II. INITIAL CALIBRATION

The purpose of the initial calibration is to exhaustively test each active element of the array to quantify its excitation levels. Two techniques are studied in this paper, park and probe, and mutual coupling-based, which will be described in the following sections.

### A. PARK AND PROBE

The park and probe technique has been traditionally used to estimate the phase and amplitude errors among all antenna elements of a phased array system [10]. The procedure is

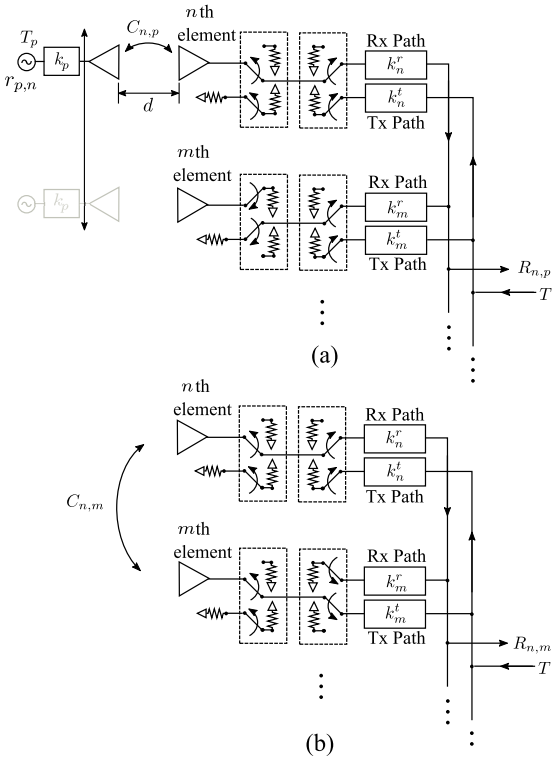


**FIGURE 1. Coupling diagram for calibration measurements in arrays with analog beamformer networks. (a) Coupling using an external antenna probe. Test the *n*th element in receive. (b) Coupling between antenna elements within the array. Transmit from *m*, receive with *n*. Both cases require the elements that are not tested to be terminated.**

straight forward, it employs a robotic manipulator to position an external antenna probe at a distance $d$ of the $n$th active element, and then proceeds to test it. The tested $n$th element is excited to its default state, and all the other elements are terminated to their corresponding transmission line impedance, as shown in Fig.1(a). Afterwards, the robotic manipulator positions the probe at boresight of the next $m$th element, at the same probe-to-antenna element distance $d$, and tests the $m$th antenna element under same testing conditions. It repeats this procedure until all elements are tested, hence the denomination ''park and probe''. It requires a robotic manipulator to precisely position the probe at broadside of each antenna element, as a consequence it can only be carried out indoors.

Since the technique tests all antenna elements under the same conditions, i.e., the probe and the antenna element are aligned at boresight at the same separation distance $d$ for any $n$th element in the array, the technique assumes that the coupling between the probe and the $n$th element, $C_{n,p}$, is the same for all $N$ elements of the array [18], i.e.,

$$C_{n,p} = C_{m,p}, \tag{1}$$

for $m = 1, \ldots, N$.

The signal path of a receive and a transmit measurement is depicted in Fig. 1. The resultant signal received by the $n$th element, $R_{n,p}$, can be formulated as

$$R_{n,p} = k_n^r C_{n,p} k_p T_p, \tag{2}$$

$k_p$ and $k_n$ being the errors associated to the electrical path of the signal in the probe and the $n$th element, respectively. The term $k_n$ lumps together the effect of the active component as well as the effect of transmission lines, antenna and analog beamformer. The super-indexes $t$ and $r$ indicate that the value corresponds to the transmit or receive path. Finally, $T_p$ indicates the incident signal which will be transmitted by the probe.

Analogously, one can formulate the received signal by the probe, $r_{p,n}$, transmitted from the $n$th element as,

$$r_{p,n} = k_p C_{n,p} k_n^t T. \tag{3}$$

Also, since the antenna coupling considered in this work is between passive antennas, the reciprocity property is considered to be present, hence, $C_{a,b} = C_{b,a}$.

The objective is to calculate the error ratios, $K^r$ and $K^t$, among the elements in receive and transmit modes, respectively. To accomplish this, a reference element is arbitrarily chosen, which will be used to normalize all ratios with respect to it. The complex ratio $K_n^r$ in receive mode, representing the amplitude and phase variation, in receive, of the $n$th element with respect to the reference $ref$, is calculated as

$$K_n^r = \frac{R_{n,p}}{R_{ref,p}}. \tag{4}$$

Using (1), (2), and defining the transmitted signal $T_p$ from the probe to be the same for all tests, (4) results in,

$$K_n^r = \frac{k_n^r}{k_{ref}^r}, \tag{5}$$

In an analog manner, it is possible to define the complex ratio $K_n^t$ in transmit mode as

$$K_n^t = \frac{r_{p,n}}{r_{p,ref}}, \tag{6}$$

Using (1) and (3) in (6) yields

$$K_n^t = \frac{k_n^t}{k_{ref}^t}. \tag{7}$$

Equations (4) and (6) are calculated from measured quantities, and they provide a complex value that relates any $n$th element to the arbitrary selected reference. Therefore, these equations allow to estimate the unknown misalignment across the array.

### B. MUTUAL COUPLING-BASED

The mutual coupling-based calibration used in this work is the one proposed by Bekers *et al.* [19] and formulated by Mitchell [24]. The main advantage of the selected approach is that it provides a mathematical framework that estimates the misalignment, by least square method, in transmit and receive, using as much information as it is available. This contrasts with the techniques proposed by [16] and [18],

which do not propose a systematic methodology to use the redundant information provided by the coupling between all the elements, which renders the approach by Bekers *et al.* more accurate than other options.

To introduce the approach it is necessary to formulate the mutual coupling measurements using the coupling diagram shown in Fig. 1(b). In a similar fashion as (2), a mutual coupling measurement consisting of a signal transmitted from the element $m$ and received by $n$, is formulated as,

$$R_{n,m} = k_n^r C_{n,m} k_m^t T, \tag{8}$$

The term $R_{n,m}$ refers to the received signal by element $m$, transmitted by $n$. Notice that the original signal $T$ is always contaminated by the transmit and receive error terms inherent to a microwave electrical path. Furthermore, the transmit/receive order is non-commutative, meaning that in general $R_{n,m} \neq R_{m,n}$. Consequently, swapping the transmit element with the receive element will produce a different pair, containing new information.

The goal of the approach is also to compute the error ratios $k_n/k_{ref}$ between all active elements and a reference, *ref*, just as the park and probe. This is accomplished by sampling active elements using neighboring elements, as opposed to park and probe that uses the probe to test all elements. As a result, there is no longer a probe that can be used as a global reference; the error ratios $k_n/k_{ref}$ must be calculated by processing coupling measurements alone. In this context, the procedure can be seen as a guide describing which pair of elements should be chosen for sampling, and formulating the equations to isolate the transmit and receive errors from the coupling samples.

The essence of the approach is based in the assumption that coupling between neighboring symmetrically disposed pair of elements have same values [19]. For this the first step is to define coupling sets consisting of pairs of antenna elements with approximately equal coupling; i.e., for an equidistant square lattice, all pairs of elements that are immediate neighbors in a row constitute the [1,0] set, and all pairs of elements that are immediate neighbors in a column constitute the [0,1] set. These sets, and other sets that can be defined are depicted in Fig. 2.

The following step is to identify combinations of two pairs within same sets and calculate ratios. For instance, for the subarray shown in Fig. 2, within the set [1,0], one could choose the pair {0, 1} and compare it to {1, 2}, by assuming that they have approximately the same coupling. The computed ratio is,

$$\frac{R_{0,1}}{R_{1,2}} = \frac{k_0^r C_{0,1} k_1^t T}{k_1^r C_{1,2} k_2^t T} = \frac{k_0^r k_1^t}{k_1^r k_2^t}, \tag{9}$$

It follows from (9), that the ratio contains information of only the unknown errors.

In order to isolate the error terms from the ratios calculated using (9), the technique suggests to linearize all ratios by reformulating their complex terms in magnitude, by using logarithms or by transforming to dB units, and in phase,

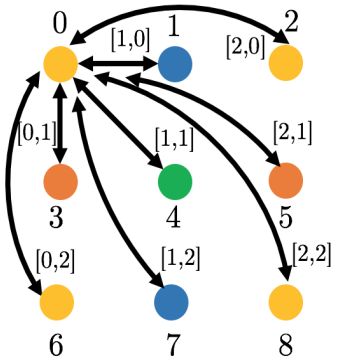


**FIGURE 2.** Depiction of coupling sets. For the mutual coupling-based initial technique proposed by [19], the couplings that belong to the same set are assumed to be of the same value.

by calculating their angle argument. In this context, it is possible to create two linear equation systems of the form [24],

$$\begin{bmatrix} 1 & -1 & 0 & 0 & 1 & -1 \\ & & \vdots & & & \end{bmatrix} \begin{bmatrix} (k_0^r)_{dB} \\ (k_1^r)_{dB} \\ (k_2^r)_{dB} \\ (k_0^t)_{dB} \\ (k_1^t)_{dB} \\ (k_2^t)_{dB} \end{bmatrix} = \begin{bmatrix} (R_{0,1})_{dB} - (R_{1,2})_{dB} \\ \vdots \end{bmatrix} \tag{10}$$

$$\begin{bmatrix} 1 & -1 & 0 & 0 & 1 & -1 \\ & & \vdots & & & \end{bmatrix} \begin{bmatrix} \angle k_0^r \\ \angle k_1^r \\ \angle k_2^r \\ \angle k_0^t \\ \angle k_1^t \\ \angle k_2^t \end{bmatrix} = \begin{bmatrix} \angle R_{0,1} - \angle R_{1,2} \\ \vdots \end{bmatrix} \tag{11}$$

The $\angle$ operator retreives the phase of a complex value, and the $(\cdot)_{dB}$ operator refers to,

$$(x)_{dB} = 20 \log_{10}(|x|). \tag{12}$$

The sparse matrix on the left side of (10), $\mathbf{A}$, is the same as the one in (11). Each row of the sparse matrix is composed of 1s and $-1$s, which represent the error terms that are in the numerator and denominator, respectively, of the linearized ratio. The number of rows of (10) and (11) depends on the number of previously defined pair combinations to process, while the number of columns is equal to the total number of unknown $k_n^r$ and $k_n^t$ terms involved. The column matrix that contains the unknown error terms is denominated $\mathbf{K}$. Lastly, the column matrix on the right side is $\mathbf{R}$, and it is composed of the measured coupling values $R_{n,m}$. Consequently, (10) and (11) have the following form:

$$\mathbf{AK} = \mathbf{R}. \tag{13}$$

The objective is now to calculate the ratios $K_n^r$ and $K_n^t$ from (10) and (11). One way to accomplish this, is to choose a

reference element and define,

$$k^r_{ref} = k^t_{ref} = 1, \tag{14}$$

which is the same as normalizing the errors with respect to the reference. In this way, (5) and (7) are simplified to $K^r_n = k^r_n$ and $K^t_n = k^t_n$. As a consequence, by calculating the $k^r_n$ and $k^t_n$ terms from (10) and (11), the unknown $K^r_n$ and $K^t_n$ ratios are also obtained. Moreover, (14) also results in

$$\angle k^r_{ref} = \angle k^t_{ref} = (k^r_{ref})_{dB} = (k^t_{ref})_{dB} = 0. \tag{15}$$

To solve (10) and (11) for $k_n$, Mitchell [24] proposed to split matrices $\mathbf{A}$ and $\mathbf{K}$ to reshape (13) into,

$$\mathbf{GK_1} + \mathbf{BK_2} = \mathbf{R}. \tag{16}$$

$\mathbf{G}$ is the sparse matrix $\mathbf{A}$ without the columns corresponding to $k^r_{ref}$ and $k^t_{ref}$, while $\mathbf{B}$ is a two column matrix formed by the two columns removed from $\mathbf{A}$. $\mathbf{K}_1$ is the column matrix $\mathbf{K}$ without $k^r_{ref}$ and $k^t_{ref}$ terms, and $\mathbf{K}_2$ is a column matrix formed solely by $k^r_{ref}$ and $k^t_{ref}$. Notice that $\mathbf{K}_1$ contains all the unknown variables; hence, to finally obtain the errors it is necessary to solve (16) for $\mathbf{K}_1$:

$$\mathbf{K_1} = \mathbf{G^{-1}}(\mathbf{R} - \mathbf{BK_2}). \tag{17}$$

$\mathbf{G}^{-1}$ is the pseudo inverse of $\mathbf{G}$.

For instance, if element 2 is chosen as a *ref*, and taking (15) into account, (10) and (11) can be rewritten according to (17) as

$$\begin{bmatrix} (k^r_0)_{dB} \\ (k^r_1)_{dB} \\ (k^t_0)_{dB} \\ (k^t_1)_{dB} \end{bmatrix} = \begin{bmatrix} 1 & -1 & 0 & 1 \\ & \vdots & & \end{bmatrix}^{-1} \begin{bmatrix} (R_{0,1})_{dB} - (R_{1,2})_{dB} \\ \vdots \end{bmatrix}, \tag{18}$$

$$\begin{bmatrix} \angle k^r_0 \\ \angle k^r_1 \\ \angle k^t_0 \\ \angle k^t_1 \end{bmatrix} = \begin{bmatrix} 1 & -1 & 0 & 1 \\ & \vdots & & \end{bmatrix}^{-1} \begin{bmatrix} (R_{0,1})_{dB} - (R_{1,2})_{dB} \\ \vdots \end{bmatrix}. \tag{19}$$

Notice that there is no $\mathbf{BK_2}$ term in (18) or (19); this is because the error terms for the reference are zero, as specified by (15).

## III. IN-SITU CALIBRATION

In contrast to initial calibration, which is often performed indoors and under controlled environmental conditions, the in-situ calibration is periodically performed on the field, during operation of the system. Its objective is to regularly monitor the status of the active elements of the array, and take corrective actions in case errors are detected. The mutual coupling-based technique detailed on Section II-B is a valid option for in-situ calibration. However, the large number of coupling measurements required and the high computational load imposed may increase testing and data processing time, making this technique less attractive for periodical monitoring of arrays with an analog beamformer, because system operation will be interrupted for longer periods of time. Moreover, the original mutual coupling-based technique proposed by Aumann *et al.* [16] and its variations [17], [18] are also great options for in-situ calibration of fielded large arrays, and they require less coupling samples than the improved version proposed by Bekers *et al.* Nonetheless, all of these techniques rely on the assumption that coupling between an antenna element and its neighbors is the same for all elements along the array, which does not hold for small arrays due to unwanted edge effects.

On the other hand, there exists another approach that avoids the equal coupling assumption between neighboring elements, therefore making it an attractive option for in-situ calibration of both small and large arrays. The approach can be introduced as a before/after comparison. First, the status of the array when it has been initially calibrated is sampled and properly stored as a "before" status. Next, during operation, the same samples are repeated, obtaining an "after" state, which is compared to the before status. The ratio between the after and before status will quantify the changes suffered by the electrical path of the active elements. Still, the before/after approach does imply the assumption that the employed sampling coupling mechanism does not change in time, i.e., the coupling between two antenna elements $C_{n,m}$ is the same when taken during initial calibration and while fielded operation.

Examples of the before/after approach are proposed in [18], [22], which employ one or more embedded elements dedicated only to monitor the operation of the active elements. However, the use of embedded elements is also subject to dynamic range issues, i.e., an embedded element may not be able to test elements far away from it with enough signal-to-noise ratio. In the case of digital phased arrays, it is common practice to perform a self-calibration employing the active elements only. For instance, [23] exploits the inherent simultaneous reception on multiple elements capability of digital phased arrays to quickly test several elements per sample, and then use the redundant information collected to estimate the transmit and receive misalignment. From the analog phased arrays perspective, which can test only a pair of elements per sample, the latter approach is not efficient since it involves several coupling sampling repetitions to cover the same number of tested elements. Thus, to adapt the technique to analog cases, more effort should be directed on defining the set of coupling measurements to perform.

Keeping in mind that the goal of this work is to investigate calibration techniques on an $8 \times 8$ active phased array, the in-situ technique to test must be compatible with small arrays with analog beamformer networks. Thus, it is proposed to use a hybrid in-situ/self calibration technique that combines the before/after approach with the initial mutual coupling-based technique proposed by Şeker [18]. The reason behind using the before/after approach is to avoid errors introduced by edge effects. Also, to avoid employing dedicated elements, the coupling measurements must be performed between the active elements themselves. This motivates the use of the

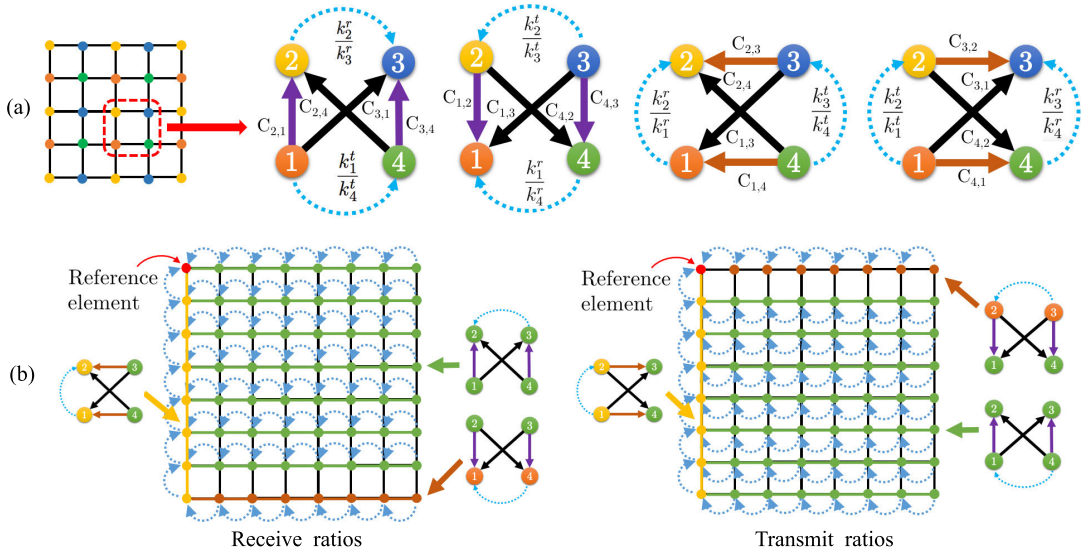


**FIGURE 3.** Coupling schemes proposed for in-situ/self calibration. (a) For any 2 × 2 subarray, performing 4 coupling measurements obtains 2 error ratios between two pairs of elements. (b) Different coupling schemes used to calculate error ratios among different pairs of elements. Adapted from [18].

technique proposed by Şeker [18], which defines the set of coupling measurements to test, and how to compute ratios from them. By performing samples among different pair of elements and avoiding using an embedded element that must test all the remaining elements, is also beneficial to avoid dynamic range issues. The following subsection will detail the proposed in-situ technique, including its limitations and benefits.

### A. ADAPTED IN-SITU/SELF CALIBRATION

As it was mentioned above, this work proposes to implement the adapted in-situ calibration technique. The technique consists of three steps:

1) After the initial calibration has been performed, sample and store a ''before", or also called factory standard, status.
2) During operation of the system, interrupt it to sample an ''after" status.
3) Compare before and after results to estimate changes on the receive and transmit modules.

To introduce the concept, the procedure is detailed in two stages. The first stage defines the coupling pairs to sample, and offers a methodology to process the collected data to obtain error ratios between antenna elements. This stage covers steps 1 and 2, and it is based on the mutual coupling-based calibration proposed by [18]. The second stage deals with the comparison procedure; it introduces the mathematical formulation to calculate the changes covering step 3.

The scheme defining the sample couplings is shown in Fig. 3(a). On the left side of the figure there is a simplified representation of a square array, and on the right side there are different coupling schemes for an arbitrarily chosen $2 \times 2$ subarray. On each scheme there are four couplings depicted; all of the them can be formulated in the same fashion as (8). For the first case, the couplings are,

$$R_{2,1} = k_2^r C_{2,1} k_1^t T, \tag{20}$$
$$R_{2,4} = k_2^r C_{2,4} k_4^t T, \tag{21}$$
$$R_{3,1} = k_3^r C_{3,1} k_1^t T, \tag{22}$$
$$R_{3,4} = k_3^r C_{3,4} k_4^t T. \tag{23}$$

In order to obtain the error ratios between elements, use (20), (21), (22) and (23), in the following expressions [18],

$$K_{3,2}^r = \sqrt{\frac{R_{2,1}R_{2,4}}{R_{3,1}R_{3,4}}} = \frac{k_2^r}{k_3^r}\sqrt{\frac{C_{2,1}C_{2,4}}{C_{3,1}C_{3,4}}}, \tag{24}$$

and,

$$K_{4,1}^t = \sqrt{\frac{R_{2,1}R_{3,1}}{R_{2,4}R_{3,4}}} = \frac{k_1^t}{k_4^t}\sqrt{\frac{C_{2,1}C_{3,1}}{C_{2,4}C_{3,4}}}. \tag{25}$$

Expression (24) calculates the receive error ratio $K_{3,2}^r$ between elements 3 and 2 multiplied by a ratio among couplings, while (25) returns the transmit error ratio $K_{4,1}^t$ between 4 and 1, also followed by a respective coupling ratio. It is convenient now to notice that the involved couplings in Fig. 3 belong to set [0,1], shown in purple, to set [1,1], in black, and to set [1,0], in red. In an ideal case, couplings within the same set are similar, thus approximating the coupling ratios on the above two expressions to 1. Therefore, (24) and (25) estimate 2 error ratios from 4 coupling measurements, and the level of accuracy depends upon how similar are same set couplings.

Nevertheless, until now only ratios between neighboring elements have been calculated, but the issue on how to relate these ratios to an arbitrary reference is unaddressed. To calculate the error ratios $K_n$ between any element and the reference element, one must define ratio paths that link the reference to

all other elements. A ratio path begins at any element and ends at the reference, and its purpose is to serve as a map indicating which ratios should calculated. For example, Fig. 3(b) shows a proposed set of ratio paths, for receive and transmit, using the top left corner element as reference. The ratio between any $n$th element to the reference is obtained as the product of all $K_{n,m}$ terms indicated in the ratio path, which is formulated as,

$$K_n^r = K_{ref,m}^r \cdots K_{q,n}^r, \tag{26}$$

and

$$K_n^t = K_{ref,m}^t \cdots K_{q,n}^t. \tag{27}$$

Indexes $m$ and $q$ represent the elements along the path.

In the context of the in-situ calibration, step 1 consists in implementing (26) and (27) immediately after the initial calibration to obtain a factory standard status set of $K_n^r|_{bef}$ and $K_n^t|_{bef}$ values, while step 2 repeats the same procedure as step 1, but at the operation location, to obtain a new set of $K_n^r|_{aft}$ and $K_n^t|_{aft}$ values. Finally, to cover step 3 and calculate the amplitude and phase deviation from the factory standard use,

$$(K_n^r)' = \frac{K_n^r|_{aft}}{K_n^r|_{bef}} = \frac{K_{ref,m}^r|_{aft} \cdots K_{q,n}^r|_{aft}}{K_{ref,m}^r|_{bef} \cdots K_{q,n}^r|_{bef}}, \tag{28}$$

and

$$(K_n^t)' = \frac{K_n^t|_{aft}}{K_n^t|_{bef}} = \frac{K_{ref,m}^t|_{aft} \cdots K_{q,n}^t|_{aft}}{K_{ref,m}^t|_{bef} \cdots K_{q,n}^t|_{bef}}. \tag{29}$$

Moreover, the assumption for this case is that couplings among elements do not change with time, i.e.,

$$C_{n,m}|_{bef} = C_{n,m}|_{aft}. \tag{30}$$

Replacing (24), (25) and assumption (30) in (28) and (29) yields,

$$(K_n^r)' = \frac{(k_n^r/k_{ref}^r)|_{aft}}{(k_n^r/k_{ref}^r)|_{bef}}, \tag{31}$$

$$(K_n^t)' = \frac{(k_n^t/k_{ref}^t)|_{aft}}{(k_n^t/k_{ref}^t)|_{bef}}. \tag{32}$$

The resultant expressions (31) and (32) calculate deviations from the original factory standard state. They must be used to track changes occurring after the system has been deployed, and they do not represent the current state by themselves. Moreover, the reference is assumed to have not suffered any change, such that $k_{ref}|_{aft} = k_{ref}|_{bef}$, which is the same assumption made in any before/after approach. The most important advantage of expressions (31) and (32) is that the coupling terms are canceled using (30) rather than the less likely assumption of equal same set coupling. Hence, there is no minimum array size imposition, and edge effects are no longer an issue for initial calibration. Another advantage is that this approach proposes a reduced number of coupling measurements, in contrast to the initial technique which requires as much information as is available.

On the other hand, there are limitations that must be considered. The square root of complex numbers in (24) and (25) produces two possible results which are 180° apart. The first result, and the one used in this work, is in the range of -90° to 90°, which means that errors larger than |90°| will be incorrectly computed. However, large phase errors are not expected to arise during operation, unless the active element antenna and/or electronics have been damaged, in which case, it should be neglected from the calibration. Also, expressions (26) and (27) are prone to error propagation, i.e., measurement errors, as noise or repeatability, are present on each $K_{n,m}$ term, and they will accumulate along the ratio path. In other words, the longer the ratio path, the greater the possibility of larger accumulated error.

## IV. EXPERIMENTAL SETUP

The C-band, 64-element, active phased array radar line replaceable unit (LRU), is the system under test (SUT) for this calibration study. The SUT is also dual-polarization capable; however, our study currently focuses on the vertical polarization. A frequency range of 5.25 to 5.45 GHz is covered by the SUT; for the experiments in this work, the operation frequency was chosen as 5.355 GHz. The T/R module architecture utilizes commercial-off-the-shelf (COTS) components [3]. The SUT is implemented using eight printed circuit boards (PCB). Each PCB consists of eight dual-polarization T/R modules, shown in Fig. 4 colored in blue. The front-end T/R module design utilizes the alternate-transmit, alternate-receive (ATAR) configuration. Each T/R module transmits a 4 W peak power at the output of the microstrip antenna patch, by means of high power amplifiers (HPAs). Each T/R module channel is equipped with a 6-bit phase shifter (PS) and a 6-bit attenuator (ATT) on the common path of transmit and receive. Furthermore, every eight T/R modules, on-board one single PCB, are combined and divided using independent beamformer networks. The on-board beamformer networks, one for receive and one for transmit, enable one element to transmit while others receive, which is the requirement for mutual coupling measurements. The eight PCBs are then externally combined using two COTS, balanced, 1-to-8 combiner/dividers, one for transmit and another for receive, as shown in Fig. 4. Depending on the calibration method chosen, the SUT is characterized using either the vector network analyzer (VNA) or the Demonstrator Radar Back end, downstream of the LRU box (colored in red).

Fig. 5 shows the exploded view of the SUT: (a) the custom anechoic chamber and scanner, (b) the LRU assembly front-end, and (c) the T/R module s. The custom chamber scanner was designed specifically for the 64-element LRU at C-band. It is capable of performing the initial characterization park and probe and near-field antenna pattern measurements. The custom chamber, lined with RF absorber, can also be configured into a microwave "quiet zone" for mutual coupling measurements. The quiet zone is achieved by covering the

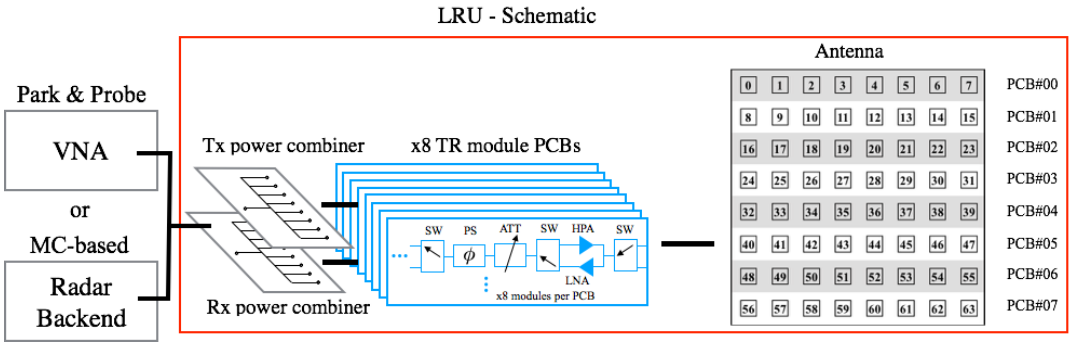


**FIGURE 4.** The schematic of the LRU assembly. The SUT utilizes analog beamforming by two levels of analog combining into one single receive channel. Inversely, it divides one analog transmit channel into the 64-element array. Each of the T/R module PCBs consist of eight (8) T/R module channels in a row, as colored in the antenna panel illustration.

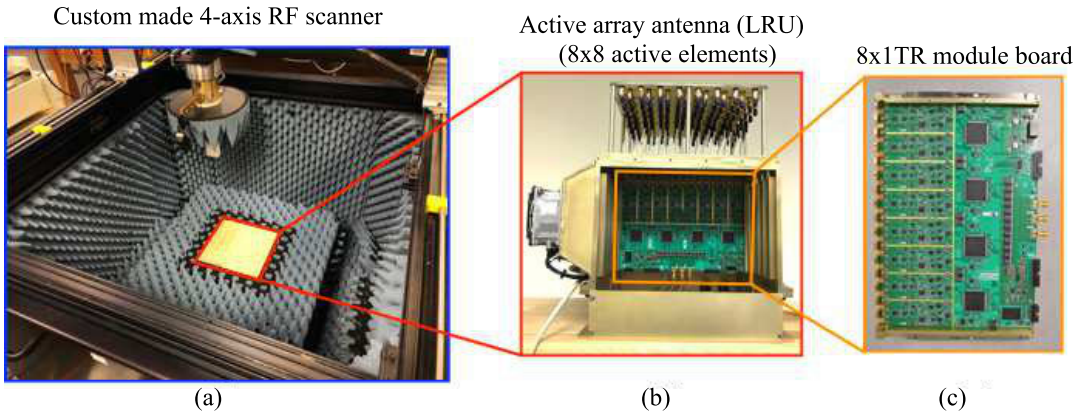


**FIGURE 5.** The LRU assembly exploded view and test setup. Each T/R module PCB (Fig. 5 (c)) consists of 8 T/R module channels. A total of 8 PCBs are installed to form an 8 × 8 active phased array radar (Fig. 5 (b)). The SUT is characterized in a custom-made, compact anechoic chamber (Fig. 5 (a)). For park and probe measurements, a 4-axis mechanical scanner is used to accurately position the open ended waveguide acting as antenna probe.

top of the scanner with another RF absorber lined metallic cover.

### A. PARK AND PROBE MEASUREMENTS

The conventional park and Probe measurement is carried out by setting the SUT inside the custom anechoic chamber as shown in Fig. 5(a). There are 3 linear actuators to provide the positioning in $x$, $y$ and $z$ directions, and a rotary table provides polarization rotation to the waveguide probe (WR-187). The waveguide probe is positioned at boresight of each antenna patch during the measurements. A VNA is employed for both the receive and transmit pulsed measurements. All measurements performed are at C-band.

### B. MUTUAL-COUPLING AND IN-SITU MEASUREMENTS

The mutual-coupling based and in-situ measurements are completed using the Radar Backend (Fig. 4 bottom measurement path). Implementing the mutual-coupling techniques using the Radar Backend expands the validation and testing of the techniques to the entire radar system. In contrast to the park and probe measurements, these measurements also include the frequency downconversion paths to baseband (70 MHz and 85 MHz). All mutual coupling measurements were performed with a RF absorber lined metallic cover on top of the scanner, to avoid reflections from the scanner.

## V. EXPERIMENTS AND RESULTS

The experiments performed in this work can be grouped into three main categories: initial calibration, in-situ calibration, and detection and diagnosis of component failure. For the initial calibrations, the techniques detailed on Section II are implemented to obtain the original misalignment of the system. The results from both park and probe and mutual coupling-based are then compared and analyzed. The experiments for the in-situ calibration forced an excitation change on some arbitrarily selected elements, and then applied the technique proposed on Section III-A to quantify the changes.

Finally, an overview of component failure cases encountered during testing is presented. The feedback data obtained from mutual coupling samples are instrumental to identify and diagnose component failure.

### A. INITIAL CALIBRATION

The performance of the two initial calibration techniques, park and probe, and Bekers' mutual coupling approach were studied. In particular, the root mean square error (RMSE)

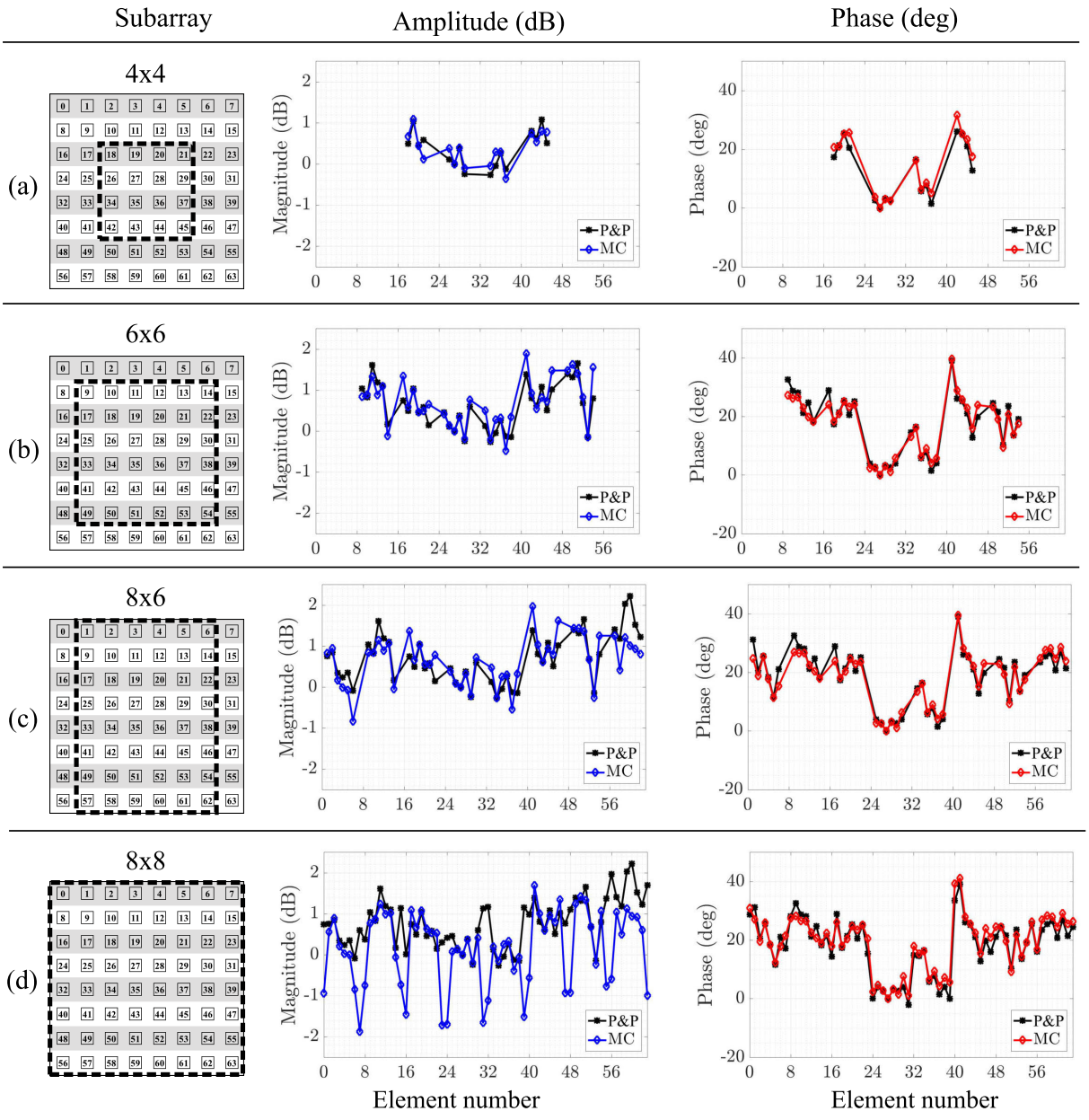


**FIGURE 6.** Estimations of the initial misalignment, in receive mode, of the SUT. The park and probe (P&P) results are compared to the ones obtained using the mutual coupling-based (MC) technique for different subarray configurations. The unwanted edge effect is most notorious on the vertical edges, affecting mostly the magnitude estimations.

of phase and amplitude were used to quantify the estimation differences between both methods. The park and probe method sampled both transmit and receive measurements of all 64 elements at a default operating point. A total of 128 samples were recorded. The error ratios between elements were computed using equations (4) and (6). On the other hand, for the mutual coupling-based technique, all measurement pairs belong to sets [0,1], [1,0], [1,1], [2,0], [0,2] and [2,1], as proposed by Bekers *et al.* [19], were collected to estimate the amplitude and phase errors. A total of 780 samples were used. Although a considerably larger amount of measurements were needed compared to the park and probe, the mutual coupling-based technique requires no mechanical movement, which significantly reduces the total testing time.

An important consideration of Bekers' mutual coupling technique is the edge effect. Antenna elements located at the edges of the array are exposed to a different environment than those located at the middle of the array, which causes their coupling values to vary, thereby compromising the assumption that couplings within the same set are equal. Simulations performed by Beckers *et al.* [19] indicate that

**TABLE 1.** Summary of RMSE of the mutual coupling-based initial calibration approach in reception and transmission.

| Subarray | Reception - $K_n^r$ | | Transmission - $K_n^t$ | |
|---|---|---|---|---|
| | RMSE amplitude (dB) | RMSE phase (deg) | RMSE amplitude (dB) | RMSE phase (deg) |
| 4×4 | 0.27 | 2.66 | 0.39 | 2.76 |
| 6×6 | 0.36 | 2.67 | 0.51 | 2.51 |
| 8×6 | 0.46 | 2.50 | 0.52 | 2.50 |
| 8×8 | 1.11 | 2.47 | 1.07 | 2.39 |

**TABLE 2.** Summary of the excitations changes, estimations, and RMSE obtained during in-situ calibration experiments.

| Reception - $(K_n^r)'$ | | | | | | |
|---|---|---|---|---|---|---|
| Element | Amplitude (dB) | | | Phase (deg) | | |
| | Value | Estimation | Error | Value | Estimation | Error |
| 4 | -2.91 | -2.89 | -0.02 | -23.30 | -23.03 | -0.27 |
| 28 | -1.16 | -1.13 | -0.03 | 21.60 | 21.70 | -0.10 |
| 32 | -1.88 | -1.87 | -0.01 | 29.38 | 29.90 | -0.52 |
| 45 | -1.97 | -1.97 | -0.00 | 2.15 | 2.12 | 0.03 |
| 46 | -2.37 | -2.31 | -0.06 | 18.20 | 18.13 | 0.07 |
| 63 | -2.04 | -2.05 | 0.01 | -7.73 | -7.61 | -0.12 |
| RMSE | 0.03 | | | 0.25 | | |
| Transmission - $(K_n^t)'$ | | | | | | |
| Element | Amplitude (dB) | | | Phase (deg) | | |
| | Value | Estimation | Error | Value | Estimation | Error |
| 15 | -1.03 | -1.07 | 0.04 | -8.01 | -8.04 | 0.03 |
| 28 | -0.97 | -1.14 | 0.17 | 22.50 | 21.10 | 1.38 |
| 29 | 0.18 | 0.37 | -0.19 | -5.53 | -5.35 | -0.18 |
| 32 | -0.02 | -0.12 | 0.10 | -8.80 | -9.70 | 0.90 |
| 54 | -1.58 | -1.66 | 0.08 | 12.70 | 11.92 | 0.78 |
| 56 | -1.94 | -2.05 | 0.11 | 22.30 | 22.28 | 0.02 |
| RMSE | 0.12 | | | 0.75 | | |

estimation errors for an 8 × 8 array are low, e.g., on the order of 0.16 dB and 2.1°. Yet, the simulations assumed an array with an infinite ground plane, which is not a reality. Consequently, the impact of the discontinuities occasioned by the finite nature of physical arrays is unknown, and it is particularly more relevant for the case of a small 8 × 8 array [26].

In order to properly assess the accuracy of the technique, it is necessary to investigate subarray arrangements with different sizes. A total of four different configurations were considered, as shown in the leftmost column in Fig. 6. For the first two cases, edge elements were avoided; for the latter cases, different edge elements were included to study the effects. To demonstrate the results of the four above-mentioned cases, the estimated $K_n^r$ in reception mode are shown in Fig. 6. The results of each case, the magnitude and phase estimations of the misalignment from the mutual coupling-based technique, are compared to the ones from park and probe, which are used as ground truth. Element 27 was chosen as the reference element for all cases because of its central location, away from the edges and relatively close to all other elements. Qualitatively, the phase estimation performs better than amplitude estimation. The summary of the RMSE, for both receive and transmit, is listed in Table 1. One can notice that the RMSE amplitude estimation worsens as the subarray gets to the edge elements. The worst result, $\text{RMSE}_{8\times8} > 1$ dB, occurs for the 8 × 8 case, which covers all edges. If compared with the 8 × 6 case, the error is reduced, $\text{RMSE}_{8\times6} \approx 0.5$ dB. This suggests that couplings on vertical edges are more perturbed than on horizontal edges for vertical polarization.

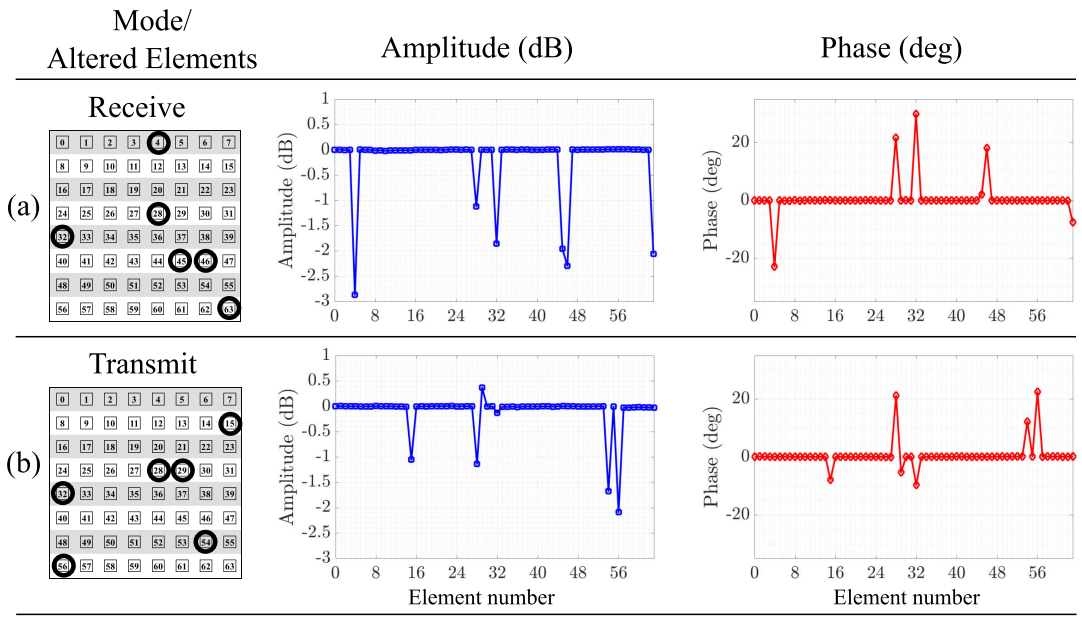


**FIGURE 7.** Estimations of the introduced changes in amplitude and phase, (a) in receive and (b) transmit mode. For each mode, the excitations of 6 elements were modified and later detected by the proposed mutual coupling-based in-situ error tracking technique.

In contrast with the magnitude estimation, the phase estimation in this particular array improves as the array size increases. However, the improvements are relatively small, 0.19 and 0.37 deg for reception and transmission, respectively. The relatively small improvement can be contributed to the effect of averaging a larger number of elements. The RMSE for all cases is close to 2.5°, which is similar to simulations, 2.1°.

In conclusion, Bekers' mutual coupling-based technique is a great option for phase estimation of misalignment in this array. However, for amplitude estimations, it is recommended to either avoid including edge elements, or add dummy elements surrounding the active ones [25]. Moreover, the estimations of errors in both transmit and receive modes are of a similar order. This should not be a surprise considering that the main source of errors of this approach are the amplitude and phase differences among the same set couplings, which were only assumed to be the same and affect both transmission and reception in a similar manner.

### B. IN-SITU CALIBRATION

The adapted in-situ/self calibration proposed in Section III-A is evaluated with a similar approach. The RMSE of both amplitude and phase, for both transmit and receive, were calculated to evaluate the performance of this technique.

A set of six arbitrarily chosen phase and amplitude values were introduced into six arbitrarily chosen elements. The phase and amplitude perturbations were introduced into the array excitation by modifying the T/R module configuration.

In order to quantify the added changes, the measurements depicted in Fig. 3 were performed. It is important to note that, instead of referencing to element 1, element 27 is used as the reference because of its central location. Next, the data set with the added perturbations was used to compute a set of $K_n^r|_{aft}$ and $K_n^t|_{aft}$ coefficients using (26) and (27), respectively. In a similar manner, to obtain a set of $K_n^r|_{bef}$ and $K_n^t|_{bef}$ values required for comparison, the data set collected during the initial calibration, (Section II-B), was used in conjunction with (26) and (27). Finally, $(K_n^r)'$ and $(K_n^t)'$ were estimated using (28) and (29).

The estimated amplitude and phase changes in receive and transmit are shown in Fig. 7. The leftmost column reflects the locations of the altered elements in the array. There are six peaks per plot, each representing the estimated value of the introduced modification. As it can be seen, the unaltered elements are prominent as their values are close to 0, which suggests no changes occurred. However, small variations within the unaltered elements are observed. The small variation can be contribution from factors such as temperature changes, measurement repeatability, non-linearity of the HPA, and low-level leakage within the T/R module channels. As a comparison, the park and probe technique was used to measure the introduced changes. The results of the comparison are detailed in Table 2. The table summarizes the comparison values, obtained using park and probe, the estimations values, calculated using the adapted in-situ technique, and the errors between them. Finally, it calculates the RMSE from the calculated errors.

The main advantage of the adapted in-situ/self calibration technique is that it greatly enhances the amplitude estimation

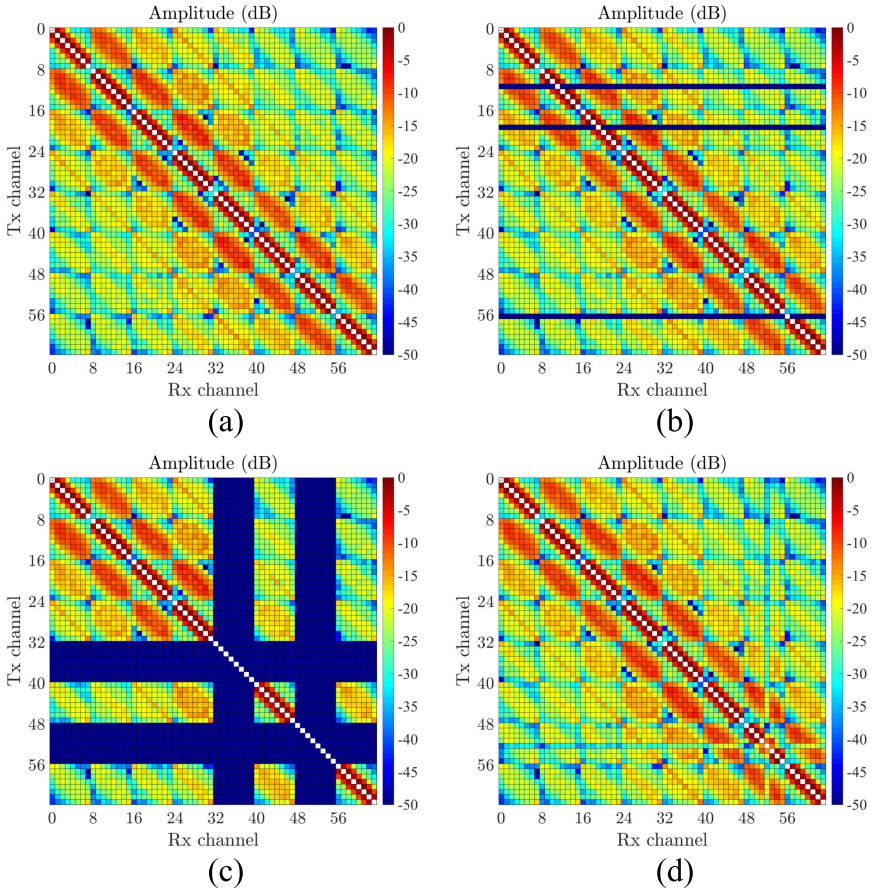


**FIGURE 8.** Examples of element failures depicted using mutual coupling measurements. Case (a) represents normal operation. Case (b) shows that elements 11, 19, and 56 fail to transmit. Case (c) depicts failure in both transmit and receive of T/R module PCBs. Finally, case (d) demonstrates a degradation in both transmit and receive on element 52.

for both cases, regardless of the location of the element. As it can be verified, the absolute value of the estimation in amplitude for any element is $< 0.19$ dB, whereas for the initial calibration case elements on the edges are underestimated by $> 1$ dB. The reason, as explained in the previous section, is that the passive coupling values are removed from the calculation by comparing the before and after states.

### C. COMPONENT FAILURE DIAGNOSIS

Mutual coupling measurements can also quickly identify component failures in a system. A collection of common failure cases, which were found over the course of the experimentation period, is presented in Fig. 8. Each of the subfigures represents the normalized measured mutual coupling amplitude of any given pair of elements. The rows of the grid indicate the transmitting element, while the columns indicate the receiving element. In other words, the values contained in the $n$th row represents the received signals by all elements that were transmitted by element $n$. Whereas the $n$th column displays the received values by element $n$, which were transmitted from all other elements. As consequence, if the entire $n$th row shows low power ($\leq$ -50 dB), then the $n$th element suffers of transmission failure. In the same manner, if the entire nth column demonstrates low power, then the $n$th element has reception problems. This rationale permits to exactly identify failed antenna elements. It is also a straight-forward observation that the amplitude of the mutual coupling decreases as the elements get further away from the transmitting element. It is important to note that the mutual coupling measurement of a given pair is taken while the rest of the elements are terminated. All measurements are taken as specified in Section II.

Fig. 8(a) demonstrates an example of a healthy $8 \times 8$ array. Fig. 8(b) shows an example of elements in transmission failure. That is, the 11th, 19th, and 56th rows in the plot indicate issues in transmit paths due, in this case, to damaged high power amplifiers. Similarly, Fig. 8(c) shows a total of 16 rows of failure in both horizontal and vertical directions, namely row 32 to 39 and 48 to 55. This suggests that the T/R module PCBs which correspond to the failed rows are neither transmitting nor receiving. It was later determined that power supplies for both PCBs were damaged.

In contrast to cases (b) and (c), with received signal levels close to the noise floor, Fig. 8(d) depicts a reduced amplitude

at both transmission and reception for element 52 (row 52 or column 52). The reduced signal level is at an alarming -10 dB, calculated by either mutual coupling-based initial or in-situ techniques. With reduction in both horizontal (transmit) and vertical (receive) directions, the symptom implies issue(s) reside in the common paths of element 52. From park and probe measurements, typical amplitude adjustments from array misalignment between all elements are ∼2.5 dB. This suggests the issue(s) are unlikely due to the array misalignment (calibration). The issue was identified to be a loose connector between the T/R module PCB and the antenna patch.

The cases demonstrated how the feedback obtained from mutual coupling measurements not only quickly identifies element failures but also provides additional information to assist system diagnosis. It is important to note that, even though the cases were illustrated using coupling data between all elements, diagnosis will be possible using a smaller amount of data. The limited amount of data collected using the in-situ mutual coupling-based technique is sufficient for system diagnosis.

Additionally, data obtained from failed components should be left out of the computation of mutual coupling-based techniques, since these techniques rely on relative ratios from element to element. Signals acquired using failed elements will bias the estimations of elements away from the reference. For this reason, before calculating the error ratios $K^t$ and $K^r$, it is necessary to check for low power signals in the same manner as discussed in the previous paragraphs, identify possible failed components, and exclude them from the calculations. Methodologies on how to avoid faulty elements have already been presented by the literature, the reader can refer to [18], [25] for more information.

## VI. CONCLUSION

The initial calibration using the mutual coupling-based technique was compared to the ones using the park and probe method. Since the mutual coupling-based technique assumes symmetrical mutual coupling between elements, the park and probe results are used as a ground truth baseline. The mutual coupling-based approach shows good estimation in phase, on the order of 2.5°, whereas the magnitude estimations are affected by edge effects, making the estimations only acceptable for element subsets chosen away from the edges. For the in-situ case, a phase and amplitude mutual coupling based monitoring technique (adapted in-situ/self-calibration) was adapted from the literature and evaluated. The monitoring technique tracks excitation changes that may arise during fielded operations, and the current state can be calculated based on the state estimated by the initial calibration stage. The main advantage of the technique is that it does not rely on the same assumptions as does its initial type counterpart, and removes the coupling values from the calculation. Hence, its misalignment estimations are more accurate, i.e., yielding in this array an RMSE less than 0.75° in-phase and less than 0.12 dB in amplitude regardless of the size of the array. A dual-polarized active 8 × 8 C-band phased subarray antenna and a fully automated 4-axis planar near-field RF scanner was used to validate the proposed calibration scheme. The diagnosis of component damage has been successfully demonstrated in real failure cases. The capability of hardware diagnosis, enabled by the mutual coupling measurements, serves a critical role in operational systems, as this capability can be utilized in the Built-in System Test (BIST) of any PAR system for operational system health monitoring.

## ACKNOWLEDGMENT

The Line Replaceable Unit (LRU) Demonstrator system has served as the development and research prototype through the validation and testing of the mutual coupling calibration techniques. Furthermore, Mr. Adam Karboski and Mr. Christopher Burghart are acknowledged for their critical support of software and firmware implementation to enable the mutual coupling technique on the radar system.

This work was supported by the National Oceanic and Atmospheric Administration (NOAA) though the Oceanic and Atmospheric Research (OAR) Office of Weather and Air Quality (OWAQ) under Grants NA170AR110333 and NA18OAR4590431. Additional support is provided from the National Science Foundation (NSF) who funds NCAR under Cooperative Agreement AGS-1852977.

## REFERENCES

[1] J. Vivekanandan, W.-C. Lee, E. Loew, J. L. Salazar, V. Grubišić, J. Moore, and P. Tsai, "The next generation airborne polarimetric Doppler weather radar," *Geosci. Instrum., Methods Data Syst.*, vol. 3, no. 2, pp. 111–126, 2014.

[2] J. Vivekanandan and E. Loew, "Airborne polarimetric Doppler weather radar: Trade-offs between various engineering specifications," *Geosci. Instrum., Methods Data Syst.*, vol. 7, no. 1, pp. 21–37, 2018.

[3] J. L. Salazar, E. Loew, P.-S. Tsai, J. Vivekanandan, W. C. Lee, and V. Chandrasekar, "Design trade-offs for airborne phased array radar for atmospheric research," in *Proc. IEEE Int. Symp. Phased Array Syst. Technol.*, Oct. 2013, pp. 371–378.

[4] M. A. Salas-Natera, R. M. Rodriguez-Osorio, and L. de Haro, "Procedure for measurement, characterization, and calibration of active antenna arrays," *IEEE Trans. Instrum. Meas.*, vol. 62, no. 2, pp. 377–391, Feb. 2013.

[5] C. Fulton, J. L. Salazar, Y. Zhang, G. Zhang, R. Kelly, J. Meier, M. McCord, D. Schmidt, A. D. Byrd, L. M. Bhowmik, S. Karimkashi, D. S. Zrnic, R. J. Doviak, A. Zahrai, M. Yeary, and R. D. Palmer, "Cylindrical polarimetric phased array radar: Beamforming and calibration for weather applications," *IEEE Trans. Geosci. Remote Sens.*, vol. 55, no. 5, pp. 2827–2841, May 2017.

[6] R. H. Medina, J. L. Salazar, E. J. Knapp, and D. J. McLaughlin, "Calibration and validation of the CASA phased array antenna," in *Proc. 42nd Eur. Microw. Conf. (EuMC)*, Oct. 2012, pp. 940–943.

[7] M. Sarcione, J. Mulcahey, D. Schmidt, K. Chang, M. Russell, R. Enzmann, P. Rawlinson, W. Guzak, R. Howard, and M. Mitchell, "The design, development and testing of the THAAD (theater high altitude area defense) solid state phased array (formerly ground based radar)," in *Proc. Int. Symp. Phased Array Syst. Technol.*, 1996, pp. 260–265.

[8] C. Fulton, J. Salazar, D. Zrnic, D. Mirkovic, I. Ivic, and D. Doviak, "Polarimetrie phased array calibration for large-scale multi-mission radar applications," in *Proc. IEEE Radar Conf. (RadarConf)*, Apr. 2018, pp. 1272–1277.

[9] R. Lebron, J. D. Diaz, and J. L. Salazar-Cerreno, "A procedure to characterize and predict active phased array antenna radiation patterns from planar near-field measurements," in *Proc. Annu. Meeting Symp. Antenna Meas. Techn. Assoc.*, 2018, pp. 1–4.

[10] J. K. Mulcahey and M. G. Sarcione, "Calibration and diagnostics of the THAAD solid state phased array in a planar nearfield facility," in *Proc. IEEE Int. Symp. Phased Array Syst. Technol.*, Oct. 1996, pp. 322–326.
[11] K. Hassett, "Phased array antenna calibration measurement techniques and methods," in *Proc. Eur. Conf. Antennas Propag.*, 2016, pp. 1–4.
[12] T. Takahashi, Y. Konishi, S. Makino, H. Ohmine, and H. Nakaguro, "Fast measurement technique for phased array calibration," *IEEE Trans. Antennas Propag.*, vol. 56, no. 7, pp. 1888–1899, Jul. 2008.
[13] S. D. Silverstein, "Application of orthogonal codes to the calibration of active phased array antennas for communication satellites," *IEEE Trans. Signal Process.*, vol. 45, no. 1, pp. 206–218, Jan. 1997.
[14] E. Lier, M. Zemlyansky, D. Purdy, and D. Farina, "Phased array calibration and characterization based on orthogonal coding: Theory and experimental validation," in *Proc. IEEE Int. Symp. Phased Array Syst. Technol. (ARRAY)*, Oct. 2010, pp. 271–278.
[15] R. Long, J. Ouyang, F. Yang, W. Han, and L. Zhou, "Multi-element phased array calibration method by solving linear equations," *IEEE Trans. Antennas Propag.*, vol. 65, no. 6, pp. 2931–2939, Jun. 2017.
[16] H. M. Aumann, A. J. Fenn, and F. G. Willwerth, "Phased array antenna calibration and pattern prediction using mutual coupling measurements," *IEEE Trans. Antennas Propag.*, vol. 37, no. 7, pp. 844–850, Jul. 1989.
[17] C. Shipley and D. Woods, "Mutual coupling-based calibration of phased array antennas," in *Proc. IEEE Int. Conf. Phased Array Syst. Technol.*, May 2000, pp. 529–532.
[18] I. Şeker, "Calibration methods for phased array radars," *Proc. SPIE*, vol. 8714, pp. 87140W-1–87140W-15, May 2013.
[19] D. Bekers, R. van Dijk, and F. van Vliet, "Mutual-coupling based phased-array calibration: A robust and versatile approach," in *Proc. IEEE Int. Symp. Phased Array Syst. Technol.*, no. 1, Oct. 2013, pp. 630–637.
[20] A. Nafe, K. Kibaroglu, M. Sayginer, and G. M. Rebeiz, "An *in-situ* self-test and self-calibration technique utilizing antenna mutual coupling for 5G multi-beam TRX phased arrays," in *IEEE MTT-S Int. Microw. Symp. Dig.*, Jun. 2019, pp. 1229–1232.
[21] K. Greene, V. Chauhan, and B. Floyd, "Built-in test of phased arrays using code-modulated interferometry," *IEEE Trans. Microw. Theory Techn.*, vol. 66, no. 5, pp. 2463–2479, May 2018.
[22] A. Agrawal and A. Jablon, "A calibration technique for active phased array antennas," in *Proc. IEEE Int. Symp. Phased Array Syst. Technol.*, Oct. 2003, pp. 223–228.
[23] C. Fulton and W. Chappell, "Calibration techniques for digital phased arrays," in *Proc. IEEE Int. Conf. Microw., Commun., Antennas Electron. Syst. (COMCAS)*, Nov. 2009, pp. 1–10.
[24] A. Mitchell, "Coupling-based wideband digital phased array calibration techniques," M.S. thesis, Univ. Oklahoma, Norman, OK, USA, 2014.
[25] Y. Neidman, R. Shavit, and A. Bronshtein, "Diagnostic of phased arrays with faulty elements using the mutual coupling method," *IET Microw., Antennas Propag.*, vol. 3, no. 2, pp. 235–241, 2009.
[26] J. L. Salazar, N. Aboserwal, J. D. Diaz, J. A. Ortiz, and C. Fulton, "Edge diffractions impact on the cross polarization performance of active phased array antennas," in *Proc. IEEE Int. Symp. Phased Array Syst. Technol. (PAST)*, Oct. 2016, pp. 1–5.

**RODRIGO M. LEBRÓN** (Student Member, IEEE) was born in Asunción, Paraguay. He received the B.S. degree in mechatronics from the Universidad Nacional de Asunción, in 2012, and the M.S. degree in mechanical engineering from the Universidade Federal do Rio Grande do Sul, RS, Brazil, in 2015. He enrolled at The University of Oklahoma, on fall 2015 on the electrical and computer engineering Ph.D. Program, where he works as a Graduate Research Assistant at the Phased Array Antenna Research and Development Group (PAARD), hosted at the Advanced Radar Research Center (ARRC). His research interests include design and development of automated systems for measurement, characterization, and calibration of phased-array antennas in microwave and mm-Wave frequencies.

**PEI-SANG TSAI** (Member, IEEE) received the B.S. degree in EE from Tamkang University, Taipei, Taiwan, and the M.S. degree in ECE from the University of Massachusetts, Amherst. After graduation, she joined the Microwave Remote Sensing Laboratory (MIRSL) and started her career in atmospheric radar development. In September 2009, she was drawn to the unique opportunity of developing an airborne, pod-based, millimeter-wave radar system, also known as the HIAPER cloud radar (HCR). She started working for the Earth Observing Laboratory (EOL), National Center for Atmospheric Research (NCAR). After HCR became operational in 2015, she transitioned her focus into the phased array radar (PAR) technology. She started her collaboration and research with The University of Oklahoma on PAR calibration and has been a key member of NCAR's Airborne Phased Array Radar (APAR) Project. Her research and work focus on development of millimeter-wave, airborne radar systems, and the calibration of phased array radars.

**JONATHAN M. EMMETT** has 25 years' experience as a Radar Technician. For the last 18 years, he has worked as a Technician for the National Center for Atmospheric Research's Earth Observing Laboratory (EOL) and has progressed into a Lead Technician for radar system developments. His radar experience ranges from S-band, X-band, Ka-band to millimeter-wave; and large-scale, dual-frequency to airborne radar systems. During the last 18 years, he has deployed these radars in 25 weather field campaigns, both domestic and international which were funded by the National Science Foundation. In 2015, his focus transitioned into phased array radar implementation and calibration. He is also the Lead Technician for EOL's LRU Demonstrator in which he led the implementation from a prototype unit to an operational radar systems. He is also a Key Contributor to the PAR calibration collaboration with The University of Oklahoma. He was responsible for the measurement implementation in the anechoic chambers.

**CALEB FULTON** (Senior Member, IEEE) received the B.S. and Ph.D. degrees in electrical and computer engineering from Purdue University, West Lafayette, IN, USA, in 2006 and 2011, respectively. He is currently an Assistant Professor in electrical and computer engineering with the Advanced Radar Research Center, The University of Oklahoma, Norman, OK, USA. He is also involved in a number of digital phased-array research and development efforts for a variety of applications. His current research interests include antenna design, digital phased-array calibration and compensation for transceiver errors, calibration for high-quality polarimetric radar measurements, integration of low-complexity transceivers and high-power GaN devices, and advanced digital beamforming design considerations. He also serves on the Education Committee of the IEEE Microwave Theory and Techniques Societies. He received the Purdue University Eaton Alumni Award for design excellence for his work on the Army Digital Array Radar Project, in 2009, the Meritorious Paper Award for a summary of these efforts from the 2010 Government Microcircuit Applications and Critical Technologies Conference, and the 2015 DARPA Young Faculty Award for his ongoing digital phased-array research.

**JORGE L. SALAZAR-CERRENO** (Senior Member, IEEE) received the B.S. degree in ECE from the University Antenor Orrego, Trujillo, Peru, the M.S. degree in ECE from the University of Puerto Rico, Mayagüez (UPRM), and the Ph.D. degree in ECE from the University of Massachusetts, Amherst, in 2011. His Ph.D. research focused on development of low-cost dual-polarized active phased array antennas (APAA). After graduation, he was awarded a prestigious National Center for Atmospheric Research (NCAR) Advanced Study Program (ASP) Postdoctoral Fellowship. At NCAR, he worked at the Earth Observing Laboratory (EOL) Division, developing airborne technology for two-dimensional, electronically scanned, and dual-pol phased array radars for atmospheric research. In July 2014, he joined the Advanced Radar Research Center (ARRC), The University of Oklahoma, as a Research Scientist, and became an Assistant Professor with the School of Electrical and Computer Engineering, in August 2015. His research interests include high-performance, broadband antennas for dual-polarized phased array radar applications, array antenna architecture for reconfigurable radar systems, APAA, Tx/Rx modules, radome EM modeling, and millimiter-wave antennas. In 2019, he was awarded the prestigious William H. Barkow Presidential Professorship from The University of Oklahoma for meeting the highest standards of excellence in scholarship and teaching. He is a Senior Member of the IEEE Antennas and Propagation Society (AP-S).